On the influence of plasma turbulence on collective Thomson scattering measurements

P Tretinnikov, E Gusakov, S Heuraux

Phys. Plasmas **30**, 032502 (2023) doi: 10.1063/5.0133213

On the influence of plasma turbulence on collective Thomson scattering measurements

P. Tretinnikov,[1,a] E. Gusakov,[1] and S. Heuraux[2]

AFFILIATIONS

[1]Ioffe Institute, 194021 Saint-Petersburg, Russia
[2]Institut Jean Lamour, 50400 Nancy, France

[a] e-mail: tretinnikov@mail.ioffe.ru

ABSTRACT

Plasma turbulence can result in significant distortion of probing and receiving microwave beams, and this effect can modify the registered spectrum in a collective Thomson scattering (CTS) experiment. An analytical description of the CTS experiment is provided in this paper for the probing beam distortion due to the plasma edge turbulence. The effect of the registered frequency spectrum distortion by the turbulence is evaluated for different turbulence levels for plasma parameters similar to those excepted in ITER.

I. INTRODUCTION

High-frequency electromagnetic beams are widely used in thermonuclear fusion research as a tool for localized plasma heating and current drive generation; for instance, the beams are used for the electron cyclotron resonance heating (ECRH) and electron cyclotron current drive (ECCD). Another application of quasi-optical electromagnetic beams in the nuclear fusion field is plasma diagnostics, possessing high spatial resolution, such as CTS and Doppler reflectometry.[1,2] The propagation of slightly divergent beams is relatively easy to analyze and predict its spatial distribution for a given plasma density and magnetic field profiles. The presence of plasma edge turbulence can significantly distort a beam launched from outside[3–8] that leads to a random distribution of the probing radiation.

The propagation of an ordinary (O-mode) and extraordinary (X-mode) polarized beam in turbulent plasma was investigated analytically and numerically in Refs. 3 and 4, respectively. It was demonstrated that the presence of a turbulent edge layer can result in a drastic distortion of a probing beam shape. The higher the turbulence amplitude is, the more significant is the distortion, and the higher the probing frequency is, the less is the effect. The developed analytical approach allowed us to describe averaged geometrical beam characteristics in turbulent plasma. Corresponding recommendation for ITER ECRH[3] and CTS[4] experiments was provided. It was also noted that this effect may lead to incorrect interpretation of the CTS registered signal,[4] but no publications on the CTS for the edge plasma turbulence are available, and the exact analysis is yet to be done. The results of the classical works devoted to the CTS analysis[9–11] can be used for the description of the experiments, where a significant spatial and angular beam broadening does not take place. The recent works about the planned CTS on ITER[12] rely upon the classical description, mostly on Ref. 10, and do not take into account the probing beam distortion due to the edge turbulence. However, as it was demonstrated in the previous research works[3–6] during the last decade that this effect is pretty pronounced even for much higher frequencies than it was planned to use for the CTS at ITER (60 GHz).

This work is devoted to the analysis of the CTS measurement interpretation with respect to the probing beam distortion due to the edge turbulence. In this work, we consider the probing beam distortions associated with the edge turbulence, implying that the edge zone contributes to a probing beam modification the most. Analytical consideration of the CTS signal in this paper is based on the method of the probing beam description in turbulent plasma developed and analyzed in detail in Refs. 3 and 4.

The paper is organized as follows: in Sec. II, we generalize the model of a probing beam description in turbulent plasma to a 3D case in the limit of small toroidal angles; this description and the introduced notations are given in Sec. III —the explicit derivation of the expression for registered power spectrum in the CTS experiment; and numerical estimates of the derived expressions are provided in Sec. IV.

II. X-MODE BEAM BROADENING IN TURBULENT PLASMA. ANALYTICAL DESCRIPTION

The propagation of a microwave beam in turbulent inhomogeneous plasma in 3D model is analyzed first. The 2D analysis was done

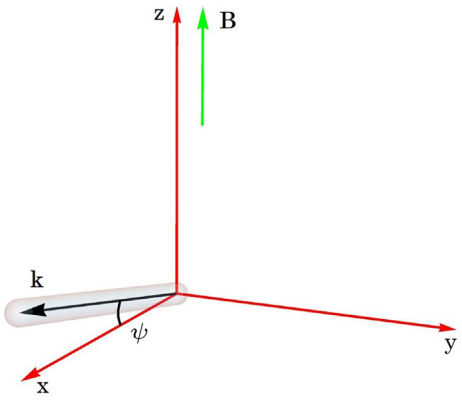

FIG. 1. Description of the probing beam at the plasma edge: the beam propagates along the wave vector **k**, which lies in the *x*–*z* plane, *x* axis is the direction of the plasma inhomogeneity, *z* axis coincides with the magnetic field vector **B**, and ψ is the angle between **k** and *x* axis.

in Ref. 4, and the key steps of that description are shortly discussed in this section together with the generalization of the description to the 3D geometry. The introduced notations will be needed for the next step—the scattered radiation analysis.

We introduce the Cartesian coordinates for the description of the beam propagation in the slab medium approximation. The slab medium model is normally applicable for description of a microwave beam propagation when the curvature of the density and magnetic field profiles is negligible on the scale of the beam width. The radial coordinate, which coincides with plasma inhomogeneity direction, is *x* axis, *z* axis corresponds to lines of external magnetic field **B**, *y* axis represents poloidal coordinate, and it is perpendicular to the *x* and *z*. The beam propagation is assumed mostly along the radial direction *x* with a small wavenumber projection on the magnetic field *z* determined by the angle ψ. The reason behind taking into account the finite angle ψ (for the emitter or receiver) is that such a geometry of a CTS experiment is used in order to avoid signals from plasma modes propagating perpendicularly to the magnetic field.[12] The discussed model of the beam propagation is illustrated in Fig. 1. The wave equation

$$\frac{\partial^2}{\partial x_j \partial x_j} E_i - \frac{\partial^2}{\partial x_i \partial x_j} E_j + \frac{\omega^2}{c^2} \varepsilon_{ij} E_j = 0 \tag{1}$$

produces the dispersion relation

$$\det \begin{vmatrix} \frac{\omega^2}{c^2}\varepsilon - k_z^2 & \frac{\omega^2}{c^2} ig & k_\perp k_z \\ -\frac{\omega^2}{c^2} ig & \frac{\omega^2}{c^2}\varepsilon - k_\perp^2 - k_z^2 & 0 \\ k_\perp k_z & 0 & \frac{\omega^2}{c^2}\eta - k_\perp^2 \end{vmatrix} = 0, \tag{2}$$

where ε_{ij} is plasma dielectric tensor, $k_\perp = \sqrt{k_x^2 + k_y^2}$ and k_z are wave vector components perpendicular and longitudinal to the magnetic field; $\varepsilon = 1 - \frac{\omega_{pe}^2}{\omega^2 - \omega_{ce}^2}$, $g = \frac{\omega_{ce}}{\omega} \frac{\omega_{pe}^2}{\omega^2 - \omega_{ce}^2}$, and $\eta = 1 - \frac{\omega_{pe}^2}{\omega^2}$ are components of the dielectric tensor in the cold-plasma approximation, where ω is probing frequency, ω_{pe} is electron plasma frequency, and ω_{ce} is electron cyclotron frequency. In expression (1) and hereafter, we assume summation over the repetitive indexes. Perpendicular wave number is the solution of the dispersion relation (2) for a given toroidal mode k_z

$$k_\perp^2(x, k_z) = \frac{\omega^2}{c^2} \frac{\varepsilon^2 - g^2 + \varepsilon\eta - (\varepsilon + \eta)\frac{c^2}{\omega^2} k_z^2}{2\varepsilon} \pm \frac{\omega^2}{c^2} \frac{\sqrt{(\varepsilon^2 - g^2 - \varepsilon\eta)^2 + 2\frac{c^2}{\omega^2} k_z^2 \left((\varepsilon + \eta)g^2 - \varepsilon(\varepsilon - \eta)^2\right) + \frac{c^4}{\omega^4} k_z^4 (\varepsilon - \eta)^2}}{2\varepsilon}. \tag{3}$$

Assuming small diffraction for a probing beam launched dominantly in the radial direction $k_x \gg k_y, k_z$ and small enough angle ψ, the expression for the radial wave number component can be simplified as

$$k_x \approx k(x) + \frac{\partial k_\perp}{\partial n} \delta n(x, y) + \frac{\partial \sqrt{k_\perp^2 - k_y^2}}{\partial k_y^2}\bigg|_{k_{y,z}=0} k_y^2 + \frac{\partial k_\perp}{\partial k_z^2}\bigg|_{k_{y,z}=0} k_z^2. \tag{4}$$

The second term is the wave number correction associated with the turbulence $\delta n(x, y)$, which normally has a dominantly perpendicular structure and is elongated in the toroidal direction, and the third and fourth terms describe the diffraction of a beam. Also, we choose the sign "+" in the expression (3) for concreteness that corresponds to the X-mode polarization, which is chosen for the CTS measurements on ITER; then, $k^2(x) = \frac{\omega^2}{c^2} \frac{\varepsilon^2 - g^2}{\varepsilon}$. The density fluctuations are taken into account in Eq. (4) in the framework of the cold plasma dispersion relation under the supposition of small wavenumber perturbation (perturbation method). This method was developed in the theory of wave propagation in the turbulent atmosphere summarized in Ref. 13. The detailed analysis of the 2D wave propagation based on the geometrical optics approach in turbulent plasma can be found in Ref. 4; here, we write down the expression for the electric field **E** distribution under the geometrical optics approximation, including the toroidal direction (3D propagation)

$$\mathbf{E}(x, y, z) = \mathbf{e} \sqrt{\frac{\omega}{ck(x)}} \int_{-\infty}^{+\infty} \int_{-\infty}^{+\infty} \frac{dk_y}{2\pi} \frac{dk_z}{2\pi} E_0(k_y, k_z) \times e^{ik_y y + ik_z z} e^{i \int_0^x dx' k(x') - i\frac{k_y^2 d_y^2(x)}{2} - i\frac{k_z^2 d_z^2(x)}{2} + i\delta\phi}, \tag{5}$$

the used notations: $d_y^2(x) = \int_0^x dx' \frac{1}{k(x')}$, $d_z^2(x) = \int_0^x dx' \frac{1}{k(x')} \left(1 - \frac{g^2(x')}{\varepsilon(x')(\varepsilon^2(x') - g^2(x') - \varepsilon(x')\eta(x'))}\right)$, the random phase $\delta\phi = -\int_0^x dx' \kappa(x') \frac{\delta n(x', y'(x, y, x', k_y))}{n(x')}$, $\kappa(x) = \frac{1}{k(x)} \frac{\omega_{pe}^2}{2c^2} \frac{(\omega^2 - \omega_{ce}^2)(\omega^2 - 2\omega_{pe}^2) + \omega_{pe}^4}{(\omega^2 - \omega_{ce}^2 - \omega_{pe}^2)^2}$,

$E_0(k_y, k_z)$ is the antenna's diagram, and $\mathbf{e}$ is the polarization vector. The four terms in the last exponent are the results of the integration of k_x (4) along the radial coordinate. It should be noted that the used approach of the beam description (5) is based on the probing beam decomposition into the partial waves, possessing the wave numbers k_y and k_z, at the plasma edge $\mathbf{E}(x=0,y,z) = \mathbf{e}\int\int_{-\infty}^{+\infty} \frac{dk_y dk_z}{4\pi^2} e^{ik_y y + ik_z z} E_0(k_y, k_z)$. This Fourier decomposition is consistent with the dispersion relation (2). Expression (5), based on supposition $k_x \gg k_y, k_z$, implies that the probing wavelength λ is much smaller than the probing beam width ρ (that is normally the case; otherwise, enormous diffraction takes place); then, the contribution of the non-propagating modes, possessing $k_{y,z} > \frac{\omega}{c}$, to the integrals in Eq. (5) is negligible. The phase perturbation of a partial wave $\delta\phi$ is the total perturbation obtained on the wave trajectory; according to the geometrical optics, the trajectory $y'(x, y, x', k_y) = y - k_y l_y^2(x', x)$, $l_{y,z}^2(x, x') = d_{y,z}^2(x) - d_{y,z}^2(x')$. If the length of the trajectory is significantly bigger than several correlation lengths, one may assume normal statistical distribution of this value. The explicit form of $E_{y0}(k_y, k_z)$ for a Gaussian diagram

$$E_0(k_y, k_z) = E 2\pi\rho^2 e^{-\frac{k_y^2\rho^2}{2}} e^{-\frac{(k_z - \frac{\omega}{c}\sin\psi)^2\rho^2}{2}}, \tag{6}$$

where $E = |\mathbf{E}(\mathbf{r}=\mathbf{0})|$, ρ is the beam width at the waist of a probing beam, and the waist is located at $x=0$ that is assumed to be around the plasma edge.

By (5), a beam passing through turbulent plasma is more perturbed the higher turbulence amplitude, and the average beam width describes this effect quantitatively. In order to define the average beam width, we consider the average intensity of the beam

$$\begin{aligned}\langle|\mathbf{E}(x,y,z)|^2\rangle = |\mathbf{e}|^2 \frac{\omega}{ck(x)} \int_{-\infty}^{+\infty}\int_{-\infty}^{+\infty} \frac{dk_{y_1}dk_{y_2}}{(2\pi)^2}\frac{dk_{z_1}dk_{z_2}}{(2\pi)^2} \\ \times E_0(k_{y_1}, k_{z_1}) E_0^*(k_{y_2}, k_{z_2}) \\ \times e^{i(k_{y_1}-k_{y_2})y} e^{i(k_{z_1}-k_{z_2})z} e^{-\frac{i\left(k_{y_1}^2-k_{y_2}^2\right)d_y^2(x)}{2}} e^{-\frac{i\left(k_{z_1}^2-k_{z_2}^2\right)d_z^2(x)}{2}} \\ \times \langle e^{i\left(\delta\phi\left(x,y,k_{y_1}\right)-\delta\phi\left(x,y,k_{y_2}\right)\right)}\rangle.\end{aligned} \tag{7}$$

The detailed analysis of the correlation function on the right-hand side of Eq. (7) is omitted (see Ref. 4); here, we provide the final expression for the average beam distribution

$$\langle|\mathbf{E}(x,y,z)|^2\rangle = |\mathbf{e}|^2 E^2 \frac{\omega}{ck(x)} \frac{\rho^2}{W_y(x)W_z(x)} e^{-\frac{y^2}{W_y^2(x)}} e^{-\frac{\left(z-\frac{\omega}{c}\sin\psi d_z^2(x)\right)^2}{W_z^2(x)}}, \tag{8}$$

the beam width components

$$\begin{aligned} W_y^2(x) &= \rho^2 + \frac{d_y^4(x)}{\rho^2} + 4\int^x D(x')l^4(x,x')dx', \\ W_z^2(x) &= \rho^2 + \frac{d_z^4(x)}{\rho^2}, \end{aligned} \tag{9}$$

the introduced function

$$D(x) = \frac{1}{2}\kappa^2(x)\frac{\delta\tilde{n}^2(x)}{n^2(x)}\int\frac{dq_y}{2\pi}|n_{0,q_y}|^2 q_y^2, \tag{10}$$

where the relative turbulence amplitude $\frac{\delta\tilde{n}^2(x)}{n^2(x)}$ and the turbulence spectrum $|n_{q_x,q_y}|^2 = \int d\Delta x d\Delta y CCF(\Delta x, \Delta y) e^{-i\Delta x q_x - i\Delta y q_y}$ are determined by the expression

$$\left\langle \frac{\delta n(x',y')}{n(x')}\frac{\delta n(x'',y'')}{n(x'')}\right\rangle = \frac{\delta\tilde{n}^2\left((x'+x'')/2\right)}{n^2\left((x'+x'')/2\right)} CCF\left(x'-x'', y'-y''\right), \tag{11}$$

where $CCF(x, y)$ is the turbulence cross-correlation function. The first term in the expression for W_y^2 (9) stands for the initial probing beam size squared, the second one represents diffraction, taking into account refractive index in inhomogeneous medium, and the third part describes the effect of the beam broadening due to the plasma turbulence. The toroidal broadening W_z^2 is described by the initial beam size and the diffraction only. The criterion for the applicability of this averaging method is enough big value of the average phase variation squared $\langle\delta\phi^2\rangle > 1$. The broadening of a microwave beam in turbulent plasma is described by the expression (9), and this characteristic of the average beam and the notations introduced during this derivation will be used in the following analysis of the average registered power in a CTS experiment.

III. CTS SIGNAL

Expressions from Sec. II describe how the edge plasma turbulence modifies the average characteristics of a probing beam; now, we continue the analysis of the beam–turbulence interaction in terms of a CTS experiment. The registered intensity in a time period T in CGS units

$$P = \frac{1}{T}\int_{-T/2}^{T/2} dt \int \mathbf{dS}\frac{c}{4\pi}|\mathbf{E}^s(t,\mathbf{r})|^2, \tag{12}$$

where $\mathbf{E}^s(t,\mathbf{r})$ is the scattered field, its intensity is integrated over the receiver waveguide cross section $\mathbf{dS}$. Applying the Wiener–Khinchin theorem, one can write the spectral power

$$\frac{dP}{d\omega^s} = \frac{1}{\pi T}\int \mathbf{dS}\frac{c}{4\pi}|\mathbf{E}_T^s(\omega^s,\mathbf{r})|^2, \tag{13}$$

where $\mathbf{E}_T^s(\omega^s,\mathbf{r}) = \int_{-T/2}^{T/2} dt e^{i\omega^s t}\mathbf{E}^s(t,\mathbf{r})$.

The CTS signal can be described based on the reciprocity theorem.[14] A Fourier amplitude of the scattered radiation, possessing the frequency ω^s, is described by the expressions

$$\mathbf{E}^s(\omega^s,\mathbf{r}) = \mathbf{E}^{\text{out}}(\mathbf{r})A(\omega^s), \tag{14}$$

$$A(\omega^s) = \frac{1}{4}\int d\mathbf{r}\mathbf{j}^{nl}(\omega^s,\mathbf{r})\mathbf{E}^+(\mathbf{r}), \tag{15}$$

where $\mathbf{E}^{\text{out}}$ is the scattered field normalized to the unit power in the registering apparatus $\frac{c}{4\pi}\int ds|\mathbf{E}^{\text{out}}|^2 = 1$, $\mathbf{E}^+ = \mathbf{e}^+E^+$ is the receiver antenna radiation normalized to the unit power as well [the index "+" is just a conventional notation from the original work,[14] and it is not related to the polarization mode in the expression (3)]. This radiation is considered in the medium with inversed sign of the magnetic field, and $\mathbf{j}^{nl}(\omega^s,\mathbf{r})$ is the Fourier transform of the source nonlinear current. The current $\mathbf{j}^{nl}$ describes bilinear interaction of the probing wave $\mathbf{E}^i = \mathbf{e}^i E^i$, possessing the frequency ω^i, with the plasma fluctuations. The vector $\mathbf{e}^{i,+}$ stands for the wave polarization. Then, the expression (13) can be written in the form

$$\frac{dP}{d\omega^s} = \frac{1}{16\pi T}\int \mathbf{dr}_1 \int \mathbf{dr}_2 E^+(\mathbf{r}_1)E^{+*}(\mathbf{r}_2) \times \int_{-T/2}^{T/2}\int_{-T/2}^{T/2} dt_1 dt_2 e^{i\omega^s(t_1-t_2)} \times \left(\mathbf{e}^+\mathbf{j}^{nl}(t_1,\mathbf{r}_1)\right)\left(\mathbf{e}^{+*}\mathbf{j}^{nl*}(t_2,\mathbf{r}_2)\right). \quad (16)$$

In the framework of the cold fluid model[10] (see the Appendix), the source current $\mathbf{j}^{nl}$ reads as

$$\mathbf{e}^+\mathbf{j}^{nl}(t,\mathbf{r}) = i\frac{e^2}{m_e}\frac{n_e}{\omega^i}\chi_\xi f_\xi^\delta(t,\mathbf{r})e^{-i\omega^i t}E^i(\mathbf{r}). \quad (17)$$

The expressions for the dimensionless parameters of the plasma fluctuations f^δ and the dimensionless vector χ are

$$f^\delta(t,\mathbf{r}) = \left\{\frac{n^\delta(t,\mathbf{r})}{n_e}, \frac{B_j^\delta(t,\mathbf{r})}{B_0}, \frac{u_j^\delta(t,\mathbf{r})}{c}\right\}, \quad (18)$$

$$\chi = \left\{\left(\mathbf{e}^+\mathbf{e}_\mu\right)\zeta_\mu, i\frac{\omega_{ce}}{\omega^s}e_{\mu\nu j}\left(\mathbf{e}^+\mathbf{e}_\mu\right)\zeta_\nu, \left(\mathbf{e}^+\mathbf{e}_\mu\right)\left(\mathbf{e}^i\mathbf{e}_j\right)\frac{ck_\mu^i}{\omega^s} - \left(\mathbf{e}^+\mathbf{e}^i\right)\frac{ck_j^i}{\omega^s} + \left(\mathbf{e}^+\mathbf{e}_j\right)\zeta_\mu\frac{ck_\mu^i}{\omega^i}\right\}, \quad (19)$$

where $\zeta_x = \frac{\omega^i}{\omega^{i2}-\omega_{ce}^2}(\omega^i\mathbf{e}_x + i\omega_{ce}\mathbf{e}_y)\mathbf{e}^i$, $\zeta_y = \frac{\omega^i}{\omega^{i2}-\omega_{ce}^2}(-i\omega_{ce}\mathbf{e}_x + \omega^i\mathbf{e}_y)\mathbf{e}^i$, and $\zeta_z = \mathbf{e}_z\mathbf{e}^i$. Here, the vectors $\mathbf{e}_\mu$ with a low index denote unit vectors with $\mu \in \{x,y,z\}$. The two vectors (18) and (19) have seven dimensions, and the index j numerates the spatial coordinates $j \in \{x,y,z\}$. It should be noted that the source current $\mathbf{j}^{nl}$ can be written in a number of ways due to linear relations between the fluctuating characteristics. The fields $\mathbf{E}^+$ and $\mathbf{E}^i$ are described for the edge turbulence according to Eqs. (5) and (6) as

$$\mathbf{E}^{i,+}(x,y,z) = \mathbf{e}^{i,+}E^{i,+}2\pi\rho^{i,+2}\sqrt{\frac{\omega^i}{ck(x)}}e^{i\int^x dx' k(x')}\int_{-\infty}^{+\infty}\int_{-\infty}^{+\infty}\frac{dk_y}{2\pi}\frac{dk_z}{2\pi} \times e^{ik_y y + ik_z z}e^{-i\frac{k_y^2 d_y^2(x)}{2} - i\frac{k_z^2 d_z^2(x)}{2} + i\delta\phi^{i,+}}e^{-\frac{k_y^2\rho^{i,+2}}{2}} \times e^{-\frac{\left(k_z - \frac{\omega^i}{c}\sin\psi^{i,+}\right)^2\rho^{i,+2}}{2}}. \quad (20)$$

It is worth mentioning that the angle between the probing (or receiving) direction and the magnetic field is $90^\circ - \psi^{i,+}$, so small values of $\psi^{i,+}$ mean almost perpendicular propagation. In this expression, the reference systems are different and associated with an emitter ($\mathbf{E}^i$) and receiver ($\mathbf{E}^+$) antennas, respectively, and the x and y coordinates stand for the probing and poloidally perpendicular to the probing directions. In equation (20), we assumed small frequency shift $\omega^s - \omega^i \ll \omega^i$, so $k(x) = k(x,\omega^i) \approx k(x,\omega^s)$.

The presence of the edge turbulence leads to distortion of the beams $\mathbf{E}^{i,+}$; hence, the spectral power becomes a random value as a function of the edge turbulence parameters. Now, we consider its average characteristic. Normally, positions of emitter, receiver, and domain of the beams cross section are separated by distances larger than the turbulence correlation length; then, the density fluctuations near the receiving and probing antennas and the fluctuations f^δ are mutually independent. To continue the analysis of the power spectrum, we introduce the following definition:

$$f_\xi^\delta(\omega,\mathbf{r}) = \int_{-T/2}^{T/2} dt f_\xi^\delta(t,\mathbf{r})e^{i(\omega^s-\omega^i)t}, \quad (21)$$

where $\omega = \omega^s - \omega^i$, and these fluctuating parameters are assumed to be statistically homogeneous in the beams intersection area, so $\langle f_\xi^\delta(\omega,\mathbf{r}_1)f_{\xi'}^{\delta*}(\omega,\mathbf{r}_2)\rangle$ is a function of $(\omega, \mathbf{r}_1 - \mathbf{r}_2)$. Taking into account all the introduced definitions and assumptions, the spectral power can be written as follows:

$$\frac{d\langle P\rangle}{d\omega^s} = \frac{r_e^2 n_e c^4}{16\pi}\frac{\chi_\xi\chi_{\xi'}^*}{\omega^{i2}}\int\frac{\mathbf{dq}}{(2\pi)^3}S_{\xi\xi'}(\omega,\mathbf{q}) \times \int\mathbf{dr}_1\int\mathbf{dr}_2\langle E^+(\mathbf{r}_1)E^{+*}(\mathbf{r}_2)\rangle\langle E^i(\mathbf{r}_1)E^{i*}(\mathbf{r}_2)\rangle e^{i\mathbf{q}(\mathbf{r}_1-\mathbf{r}_2)}, \quad (22)$$

where $r_e^2 = \frac{e^4}{m_e^2c^4}$ and the fluctuation spectrum $S_{\xi\xi'}(\omega,\mathbf{q})$ introduced according to the Wiener–Khinchin theorem

$$\int\frac{\mathbf{dq}}{(2\pi)^3}S_{\xi\xi'}(\omega,\mathbf{q})e^{i\mathbf{q}(\mathbf{r}_1-\mathbf{r}_2)} = \frac{n_e}{T}\langle f_\xi^\delta(\omega,\mathbf{r}_1)f_{\xi'}^{\delta*}(\omega,\mathbf{r}_2)\rangle. \quad (23)$$

To evaluate the double integral over space in Eq. (22), we introduce perpendicular structure of the fields $E_\perp^{i,+}(\mathbf{r}) = E^{i,+}(\mathbf{r})e^{-i\int^{\mathbf{r}}d\mathbf{r}'\mathbf{k}^{i,+}(\mathbf{r}')}$, where $\mathbf{k}^{i,+}$ are the wave vectors of the two beams, the integral is taken along each of the wave vectors $\mathbf{k}^{i,+}$, and the residual wave vector $\mathbf{\Delta k} = \mathbf{q} + \mathbf{k}^i + \mathbf{k}^+$, and then,

$$\frac{d\langle P\rangle}{d\omega^s} = \frac{r_e^2 n_e c^4}{16\pi}\frac{\chi_\xi\chi_{\xi'}^*}{\omega^{i2}}\int\frac{\mathbf{dq}}{(2\pi)^3}S_{\xi\xi'}(\omega,\mathbf{q})\int\mathbf{dr}_1\int\mathbf{dr}_2\langle E_\perp^+(\mathbf{r}_1)E_\perp^{+*}(\mathbf{r}_2)\rangle \times \langle E_\perp^i(\mathbf{r}_1)E_\perp^{i*}(\mathbf{r}_2)\rangle e^{i\int^{\mathbf{r}_1}\mathbf{dr}'\mathbf{\Delta k}(\mathbf{r}')-i\int^{\mathbf{r}_2}\mathbf{dr}'\mathbf{\Delta k}(\mathbf{r}')} \quad (24)$$

The expression $\mathbf{\Delta k}(\mathbf{r}=\mathbf{0}) = \mathbf{0}$ determines the main resolved fluctuation wave vector (Bragg's condition), position $\mathbf{r} = \mathbf{0}$ is the point of the beam axis cross section [here, we introduce a new local reference system, the description of the beams (20) in this system will be provided further], that is why as a rule the main contribution to the integral over the fluctuation wave vector $\mathbf{q}$ comes from the vicinity of $\mathbf{q} = -\mathbf{k}^i - \mathbf{k}^+|_{\mathbf{r}=\mathbf{0}}$. The wave vectors $\mathbf{k}^i$ and $\mathbf{k}^+$ are set by geometry of an experiment and the refraction. The symbolic expression $\int^{\mathbf{r}_{1,2}}\mathbf{dr}'\mathbf{\Delta k}(\mathbf{r}')$ represents sum of integrals along each of the three wave vectors. To calculate (24), we introduce local Cartesian coordinates system, where x axis corresponds to the direction of the probing beam, and y axis is perpendicular to x and external magnetic field (z axis). The beam from the receiver (imaginary) crosses the probing one at the angle $\alpha = \angle(\mathbf{k}_\perp^i, \mathbf{k}_\perp^+)$ in the perpendicular cross section. The angle α is determined not only by the boundary conditions but also by the propagation in plasma as well. The scattering angle in the toroidal direction is $\psi^i + \psi^+$ according to the model. Even though the two beams do not propagate straightforward, we assume their rectilinear propagation on the scale of the intersection area, also neglecting their diffraction on this scale. Also, we assume that the density profile is a function of x only, and this assumption is based on the fact that the probing beam in a CTS experiment is usually launched radially so that the measurements provide information from different magnetic surfaces. In addition, it is assumed that the variation of wave vectors on the scale of the beam cross section is caused dominantly by the variation of the density rather than the magnetic field that is normally the case

when a cutoff or upper-hybrid resonance is outside of the probing volume. Under these assumptions, $\mathbf{k}^{i,+}(\mathbf{r}) = \mathbf{k}^{i,+}(x)$. The explicit form for the symbolic expression $\int^{\mathbf{r}} \mathbf{dr}' \mathbf{\Delta k}(\mathbf{r}')$ in the discussed geometry is

$$\int^{\mathbf{r}} \mathbf{dr}' \mathbf{\Delta k}(\mathbf{r}') = \int^{x} dx' \left(k(x') + q_x\right) + q_y y + \left(q_z + \frac{\omega^i}{c}\left(\sin\psi^i + \sin\psi^+\right)\right) z + \int^{\cos\alpha x + \sin\alpha y} dx' k\left(\sin^2\alpha x - \sin\alpha\cos\alpha y + \cos\alpha x'\right), \tag{25}$$

and the perpendicular structure of the fields

$$E^i_\perp(x,y,z) = E^i 2\pi\rho^{i2}\sqrt{\frac{\omega^i}{ck(x)}} e^{-i\frac{\omega^i}{c}\sin\psi^i z} \int_{-\infty}^{+\infty}\int_{-\infty}^{+\infty} \frac{dk_y}{2\pi}\frac{dk_z}{2\pi} \times e^{ik_y y + ik_z z} e^{-i\frac{k_y^2 l_y^{i2}}{2} - i\frac{k_z^2 l_z^{i2}}{2} + i\delta\phi^i} e^{-\frac{k_y^2\rho^{i2}}{2}} e^{-\frac{\left(k_z - \frac{\omega^i}{c}\sin\psi^i\right)^2\rho^{i2}}{2}},$$

$$E^+_\perp(x,y,z) = E^+ 2\pi\rho^{+2}\sqrt{\frac{\omega^i}{ck(x)}} e^{-i\frac{\omega^i}{c}\sin\psi^+ z} \int_{-\infty}^{+\infty}\int_{-\infty}^{+\infty} \frac{dk_y}{2\pi}\frac{dk_z}{2\pi} \times e^{ik_y(\cos\alpha y - \sin\alpha x) + ik_z z} e^{-i\frac{k_y^2 l_y^{+2}}{2} - i\frac{k_z^2 l_z^{+2}}{2} + i\delta\phi^+} \times e^{-\frac{k_y^2\rho^{+2}}{2}} e^{-\frac{\left(k_z - \frac{\omega^i}{c}\sin\psi^+\right)^2\rho^{+2}}{2}}, \tag{26}$$

where $l^{i,+2}_{y,z}$ describe diffractive broadening of the radiations acquired before position of the beam cross-sectional area, $l^{i,+2}_y = \int_{l^{i,+}} \frac{ds}{k(s)}$ and $l^{i,+2}_z = \int_{l^{i,+}} \frac{ds}{k(s)}\left(1 - \frac{g^2(s)}{\varepsilon(s)(\varepsilon^2(s) - g^2(s) - \varepsilon(s)\eta(s))}\right)$, and the integration is performed along beam trajectories. It should be noted that, considering the emitter and receiver are in the same poloidal cross section, the intersection of two beams requires fulfilling the equality of the axis toroidal coordinate z, so $l^{i2}_z \frac{\omega^i}{c}\sin\psi^i = l^{+2}_z \frac{\omega^i}{c}\sin\psi^+$.

The result of the averaging for $\langle E^i_\perp(\mathbf{r}_1) E^{i*}_\perp(\mathbf{r}_2)\rangle$ gives

$$\langle E^i_\perp(\mathbf{r}_1) E^{i*}_\perp(\mathbf{r}_2)\rangle = |E^i|^2 \frac{\omega^i}{ck_0}\frac{\rho^{i2}}{W^i_y W^i_z} e^{-\frac{l^{i4}_z \frac{\omega^{i2}}{c^2}\sin^2\psi^i}{W^{i2}_z}} e^{\frac{-\left(z_1^2 + z_2^2\right) + i\left(z_1^2 - z_2^2\right)\frac{l^{i2}_z}{\rho^{i2}}}{2W^{i2}_z}} \times e^{\frac{(z_1+z_2) l^{i2}_z \frac{\omega^i}{c}\sin\psi^i - i(z_1 - z_2)\frac{l^{i4}_z}{\rho^{i2}}\frac{\omega^i}{c}\sin\psi^i}{W^{i2}_z}} e^{-\frac{(y_1+y_2)^2}{4W^{i2}_y}} \times e^{-(y_1-y_2)^2\frac{1}{4}\left(\sigma^{i2} - \frac{R^{i2}}{W^{i2}_y}\right)} e^{i\frac{1}{2}(y_1-y_2)(y_1+y_2)\frac{R^i}{W^{i2}_y}}, \tag{27}$$

and the used notations in this expression are

$$\sigma^{i,+2} = \frac{1}{\rho^{i,+2}} + 4\int_{l^{i,+}} D(x')dx', \tag{28}$$

$$R^{i,+} = \frac{l^{i,+2}_y}{\rho^{i,+2}} + 4\int_{l^{i,+}} D(x') l^{i,+2}_y(0,x')dx'. \tag{29}$$

An analogous expression can be written for $\langle E^+_\perp(\mathbf{r}_1) E^{+*}_\perp(\mathbf{r}_2)\rangle$, one just should change the indexes from "i" to "+" and the y coordinate from y to $\cos\alpha y - \sin\alpha x$. The expressions (28) and (29) are obtained in the framework of the procedure of the average phase variation $\langle(\delta\phi^{i,+}(x_1,y_1,k_{y1}) - \delta\phi^{i,+}(x_2,y_2,k_{y2}))^2\rangle$ decomposition, and the procedure is described in detail in Ref. 4. It should be mentioned that the beam widths $W^2_{y,z}$ introduced in Eq. (9) are used in Eq. (27) with the modification of $d^2_{y,z} \mapsto l^{i,+2}_{y,z}$, and this substitution accounts for the different beam diffractions up to the scattering area along their paths. The introduced parameter $\sigma^{i,+2}$ has the meaning of the angular beam broadening,[3] when the scattering area is deep into plasma beyond the turbulent layer the dimensionless parameter $R^{i,+}$ has the meaning of the path of product beam with its angular broadening $R^{i,+} \approx l^{i,+2}_y \sigma^{i,+2}$.

Scattering of a probing beam by the edge turbulence may result in an significant increase in the two beams of overlap domain. If the plasma is inhomogeneous, Bragg's rule for a fixed fluctuation mode $\mathbf{q}$ (determined in the scattering domain center $\mathbf{\Delta k}(\mathbf{r} = \mathbf{0}) = 0$) is not fulfilled in the whole scattering area. The wider the beams, the less the scattered radiation is correlated from different parts of the beam overlapping region. To take into account the plasma inhomogeneity on the scale of the beam cross section, we approximate the wave vector $k(x)$ by a linear function $k(x) = k_0 + \frac{k_0}{L}x$, where $\frac{k_0}{L} = \frac{dk}{dx}|_{x=0}$, where L is a local wave vector gradient. Then, the expression (24) reads as

$$\frac{d\langle P\rangle}{d\omega^s} = \frac{r_e^2 n_e c^4}{16\pi}\frac{\chi_\xi \chi^*_{\xi'}}{\omega^{i2}} \int \frac{\mathbf{dq}}{(2\pi)^3} S_{\xi\xi'}(\omega,\mathbf{q}) \int \mathbf{dr}_1 \int \mathbf{dr}_2 \langle E^+_\perp(\mathbf{r}_1) E^{+*}_\perp(\mathbf{r}_2)\rangle \times \langle E^i_\perp(\mathbf{r}_1) E^{i*}_\perp(\mathbf{r}_2)\rangle e^{i\left(k_0(1+\cos\alpha) + q_x\right)(x_1 - x_2) + i\left(q_y + k_0\sin\alpha\right)(y_1 - y_2) + i\left(q_z + \frac{\omega^i}{c}\left(\sin\psi^i + \sin\psi^+\right)\right)(z_1 - z_2)} \times e^{i\frac{k_0}{2L}(1+\cos\alpha+\cos\alpha\sin^2\alpha)\left(x_1^2 - x_2^2\right) - i\frac{k_0}{2L}\sin^2\alpha\cos\alpha\left(y_1^2 - y_2^2\right) + i\frac{k_0}{L}\sin^3\alpha(x_1 y_1 - x_2 y_2)}. \tag{30}$$

Summing up a description of the scattering model with all the made assumptions, the function under the double space integral in Eq. (30) represents an exponential bilinear form that is bulky nevertheless easy to calculate. The linear approximation for the wave vector $k(x)$ implies that the quadratic and the next terms of the decomposition do not play a big role, so the estimate of this applicability criterion is $L \gg \sqrt{\frac{W^{i,+3}}{\lambda_0}}$, and $\lambda_0 = \frac{2\pi}{k_0}$ is a local probing wavelength. Then, we write down the result of the integration of six mixed integrals in Eq. (30)

$$\frac{d\langle P\rangle}{d\omega^s} = P^i r_e^2 \lambda_0^{i2} n_e \frac{1}{\sqrt{W^{i2}_z + W^{+2}_z}} \frac{1}{4\pi^{3/2}|\sin\alpha|} G_{\xi\xi'} S^{eff}_{\xi\xi'}\left(\omega,\mathbf{q}^\delta\right), \tag{31}$$

where the effective turbulence spectrum

$$S^{eff}_{\xi\xi'}\left(\omega,\mathbf{q}^\delta\right) = \int \mathbf{dq} S_{\xi\xi'}\left(\omega,\mathbf{q}^\delta + \mathbf{q}\right) SCF(\mathbf{q}). \tag{32}$$

In this expression, $SCF(\mathbf{q})$ is the spectrum contribution function, and the main resolved fluctuation wave number is

$$\mathbf{q}^{\delta} = -\mathbf{e}_x k_0(1+\cos\alpha) - \mathbf{e}_y k_0 \sin\alpha - \mathbf{e}_z \frac{\omega^i}{c}\left(\sin\psi^i + \sin\psi^+\right), \quad (33)$$

which is determined by the scattering geometry, and the $G_{\xi\xi'}$ dimensionless function describes the contribution of each type of fluctuations to the spectral power

$$G_{\xi\xi'} = \chi_\xi \chi^*_{\xi'}. \quad (34)$$

The definition of the spectrum contribution function $SCF(\mathbf{q})$ is the main object of this work. This function quantitatively describes the contribution of all the fluctuation modes to the registered signal and contains parameters of the edge turbulence

$$SCF(\mathbf{q}) = \frac{\sqrt{W_z^{i2}+W_z^{+2}}}{\pi^{3/2}\sqrt{\sin^2\alpha\sigma^{i2}\sigma^{+2} + f_1\left(\frac{k_0}{L}\right)}\sqrt{\frac{W_z^{+2}}{\rho^{i2}} + \frac{W_z^{i2}}{\rho^{+2}} + 2\left(1+\frac{l_z^{i2}l_z^{+2}}{\rho^{i2}\rho^{+2}}\right)}} \times e^{-\frac{W_z^{i2}+W_z^{+2}}{\frac{W_z^{+2}}{\rho^{i2}}+\frac{W_z^{i2}}{\rho^{+2}}+2\left(1+\frac{l_z^{i2}l_z^{+2}}{\rho^{i2}\rho^{+2}}\right)}q_z^2} e^{-L_{xx}q_x^2} e^{-L_{xy}q_x q_y} e^{-L_{yy}q_y^2}. \quad (35)$$

The introduced notations are

$$L_{xx} = 8\tan^2\left(\frac{\alpha}{2}\right)\frac{\sigma^{i2}+\sigma^{+2}\cos^2\alpha + f_2\left(\frac{k_0}{L}\right)}{32\sigma^{i2}\sigma^{+2}\sin^4\left(\frac{\alpha}{2}\right) + f_5\left(\frac{k_0}{L}\right)},$$

$$L_{xy} = -8\tan\left(\frac{\alpha}{2}\right)\frac{2\sigma^{+2}\cos\alpha(\cos\alpha-1) + f_3\left(\frac{k_0}{L}\right)}{32\sigma^{i2}\sigma^{+2}\sin^4\left(\frac{\alpha}{2}\right) + f_5\left(\frac{k_0}{L}\right)}, \quad (36)$$

$$L_{yy} = \frac{32\sigma^{+2}\sin^4\left(\frac{\alpha}{2}\right) + f_4\left(\frac{k_0}{L}\right)}{32\sigma^{i2}\sigma^{+2}\sin^4\left(\frac{\alpha}{2}\right) + f_5\left(\frac{k_0}{L}\right)},$$

where $f_{1-5}\left(\frac{k_0}{L}\right)$ are polynomials of $\frac{k_0}{L}$ and $f_{1-5}(0) = 0$

$$\begin{aligned}
f_1(Q) &= Q4\cos^2\left(\frac{\alpha}{2}\right)\left[(R^+\sigma^{i2} + R^i\sigma^{+2})\cos\alpha + R^+\sigma^{i2}\sin^2\alpha\right] + Q^2\frac{\cot^2\left(\frac{\alpha}{2}\right)}{8}\\
&\times\left[-8(R^{i2}+R^{+2}) + \left(8W_y^{i2}+7W_y^{+2}\right)\sigma^{i2} + 4\left(W_y^{i2}+2W_y^{+2}\right)\sigma^{+2}\right.\\
&+4\left(2R^iR^+ + W_y^{+2}\sigma^{i2}\right)\cos\alpha + 4\left(4R^iR^+ + W_y^{i2}\sigma^{+2}\right)\cos 2\alpha\\
&\left.-4\left(2R^iR^+ + W_y^{+2}\sigma^{i2}\right)\cos 3\alpha + W_y^{+2}\sigma^{i2}\cos 4\alpha\right] - Q^3 8\cos^4\left(\frac{\alpha}{2}\right)\\
&\times\left[\left(R^+W_y^{i2} + R^iW_y^{+2}\right)\cos\alpha + R^iW_y^{+2}\sin^2\alpha\right] + Q^4\frac{1}{4}W_y^{i2}W_y^{+2}\frac{\sin^6\alpha}{\sin^4\left(\frac{\alpha}{2}\right)},\\
f_2(Q) &= -Q8R^+\sin\alpha\sin 2\alpha + Q^2 8W_y^{+2}\sin^4\alpha,\\
f_3(Q) &= Q\left[2R^i - R^+(\cos\alpha + 2\cos 2\alpha - \cos 3\alpha)\right] + Q^2 2W_y^{+2}\sin^2\alpha(\sin^2\alpha + \cos\alpha),\\
f_4(Q) &= Q4R^+(3\cos\alpha - 4\cos 2\alpha + \cos 3\alpha) + Q^2\left[8W_y^{i2} + W_y^{+2}(7 + 4\cos\alpha - 4\cos 3\alpha + \cos 4\alpha)\right],\\
f_5(Q) &= Q32\sin^2\left(\frac{\alpha}{2}\right)\left[(R^+\sigma^{i2} + R^i\sigma^{+2})\cos\alpha + R^+\sigma^{i2}\sin^2\alpha\right] + Q^2\\
&\times\left[-8(R^{i2}+R^{+2}) + \left(8W_y^{i2}+7W_y^{+2}\right)\sigma^{i2} + 4\left(W_y^{i2}+2W_y^{+2}\right)\sigma^{+2} + 4\left(2R^iR^+ + W_y^{+2}\sigma^{i2}\right)\cos\alpha\right.\\
&+4\left(4R^iR^+ + W_y^{i2}\sigma^{+2}\right)\cos 2\alpha - 4\left(2R^iR^+ + W_y^{+2}\sigma^{i2}\right)\cos 3\alpha + W_y^{+2}\sigma^{i2}\cos 4\alpha] - Q^3 16\sin^2\alpha\\
&\times\left[\left(R^+W_y^{i2} + R^iW_y^{+2}\right)\cos\alpha + R^iW_y^{+2}\sin^2\alpha\right] + Q^4 8W_y^{i2}W_y^{+2}\sin^4\alpha.
\end{aligned} \quad (37)$$

If one considers the effect of the angular beam broadening only, the spectrum contribution function $SCF(\mathbf{q})$ is way more compact and its dependence on the poloidal parameters is associated only with the average angular broadening $\sigma^{i,+2}$,

$$SCF(\mathbf{q}) = \frac{\sqrt{W_z^{i2} + W_z^{+2}}}{\pi^{3/2}\sqrt{\sin^2\alpha\sigma^{i2}\sigma^{+2}}\sqrt{\frac{W_z^{+2}}{\rho^{i2}} + \frac{W_z^{i2}}{\rho^{+2}} + 2\left(1 + \frac{l_z^{i2}l_z^{+2}}{\rho^{i2}\rho^{+2}}\right)}} \times e^{-\frac{W_z^{i2}+W_z^{+2}}{\frac{W_z^{+2}}{\rho^{i2}} + \frac{W_z^{i2}}{\rho^{+2}} + 2\left(1+\frac{l_z^{i2}l_z^{+2}}{\rho^{i2}\rho^{+2}}\right)}q_z^2} e^{-q_x^2\frac{\sigma^{i2}+\sigma^{+2}\cos^2\alpha}{\sigma^{i2}\sigma^{+2}\sin^2\alpha}} e^{-2q_xq_y\frac{\cot\alpha}{\sigma^{i2}}} e^{-\frac{q_y^2}{\sigma^{i2}}}. \tag{38}$$

The function $SCF(\mathbf{q})$ is normalized as $\int \mathbf{dq} SCF(\mathbf{q}) = 1$.

The choice of the CTS geometry (the angles α and $\psi^{i,+}$) determines the main resolved fluctuation wave number $\mathbf{q}^\delta$, often this wave vector is considered the only one which contributes to the scattered radiation. Nevertheless, since a probing beam and receiver radiation pattern possess finite angular beam broadening, it is clear that Bragg's rule is fulfilled for some range of the fluctuation wave vectors. This angular broadening is usually assumed to be negligible. For instance, $S_{\xi\xi'}(\omega, \mathbf{q})$ was considered as a slow function in the analogous expression in work[11] as Eq. (22); then, $S^{eff}_{\xi\xi'}(\omega, \mathbf{q}^\delta) \approx S_{\xi\xi'}(\omega, \mathbf{q}^\delta)$. Yet, the presence of the edge turbulence can increase the angular broadening significantly. The expression (31) describes this effect explicitly and quantitatively.

We consider the situation when only one fluctuation mode exists and possesses the wave number $\mathbf{q}^\delta$, so $S_{\xi\xi'}(\omega, \mathbf{q}) \sim \delta(\mathbf{q} - \mathbf{q}^\delta)$. Then, we can evaluate the signal damping due to the edge turbulence; to do this, we compare the scattered power for the edge turbulence and without taking into account the turbulence

$$\frac{d\langle P\rangle/d\omega^s|_{turb\neq 0}}{d\langle P\rangle/d\omega^s|_{turb=0}} = \sqrt{\frac{\sin^2\alpha\frac{1}{\rho^{i2}\rho^{+2}} + f_1\left(\frac{k_0}{L}\right)\Big|_{turb=0}}{\sin^2\alpha\sigma^{i2}\sigma^{+2} + f_1\left(\frac{k_0}{L}\right)\Big|_{turb\neq 0}}}. \tag{39}$$

This expression describes the decrease in the radiation scattered off the single mode. It is interesting that if we consider the full scattering spectrum for all the modes and the spectrum is almost a constant on the scale of $SCF(\mathbf{q} - \mathbf{q}^\delta)$ significant variations, this mitigation effect for the single mode is compensated by summation over all the other modes. This statement holds for any parameters of the turbulence and the plasma local gradient L.

As discussed in Sec. I, the analytical description of the beam propagation in the turbulent plasma is valid in the strong phase variation regime $\langle\delta\phi^2\rangle > 1$, so this criterion is required for the spectral power (31). Yet, if the phase variation is zero $\delta\phi^{i,+} = 0$ (the absence of the turbulence and the beams is not perturbed), the procedure of the spectral power averaging gives the same expression (31), where $\delta n = 0$, so it is also applicable for $\langle\delta\phi^2\rangle = 0$. Of course the expression for the spectral power was already derived and analyzed in previous works (e.g., Ref. 10), but in this case, Eq. (31) describes the dependence on the beam angular and special widths explicitly and for the local plasma gradient.

IV. ESTIMATE OF THE TURBULENCE EFFECT ON THE CTS SIGNAL

To estimate how the presence of the edge turbulence influences the effective spectrum $S^{eff}_{\xi\xi'}(\omega, \mathbf{q}^\delta)$, we evaluate the derived expression for different turbulence regimes and the scattering geometry.

The used spectrum model $S_{\xi\xi'}(\omega, \mathbf{q}) = \delta_{\xi n}\delta_{\xi' n}S_{nn}(\omega, \mathbf{q})$ [the index n in the delta function $\delta_{\xi n}$ denotes the first component of the vector (18)] and $S_{nn}(\omega, \mathbf{q}) = S_e(\omega, \mathbf{q}) + S_i(\omega, \mathbf{q}) + S_\alpha(\omega, \mathbf{q})$, where $S_{e,i,\alpha}(\omega, \mathbf{q})$ are the contribution of the electron, ion, and alpha particle components, respectively, to the scattered radiation. The analytical expressions for the electron spectral density correlation function components $S_{e,i,\alpha}(\omega, \mathbf{q})$ depend on the electrons, ions, and alpha particles of velocity distribution functions. The electrons and ions are assumed to follow the Maxwellian distribution function. Taking into account, the alpha particles are regarded in the model of the slow-down distribution function.[16] For the full explicit expression $S_{e,i,\alpha}(\omega, \mathbf{q})$ (they are quite bulky), we refer the readers to Ref. 17.

All the spectrum evaluations are fulfilled under the parameters and models listed as follows: the probing frequency $f^i = 60$ GHz, the model density profile, and edge turbulence envelope are illustrated in Fig. 2, the background density flat-top level $n_{\max} = 1.2 \times 10^{14}$ cm^{-3}. The magnetic field $B(x) = 5.1 \times \frac{600}{800-x}$ T, where x—radial coordinate is in centimeters. Density of the alpha particles is $n_\alpha = 7.5 \times 10^{11}$ cm^{-3}, the electron, and ion temperatures $T_e = T_i = 10$ keV. The turbulence cross-correlation function is Gaussian $CCF(x, y) = e^{-\frac{x^2}{l_c^2} - \frac{y^2}{l_c^2}}$ with isotropic correlation length $l_c = 1$ cm.

The first evaluation of the effective turbulence spectrum is performed for the following scattering geometry: $\alpha = 90^\circ$ and $\psi^i = \psi^+ = 15^\circ$, so the probing and receiving angels to the magnetic field are 75°. Taking into account the notations introduced, the probing beam wave vector in the scattering area $\mathbf{k}^i = \mathbf{e}_x k_0$, and the scattered beam wave vector $\mathbf{k}^s = \mathbf{k}^i + \mathbf{q}^\delta$, then the scattering angle $\theta = \angle(\mathbf{k}^i, \mathbf{k}^s) \approx 106^\circ$, and the angle between the main resolved fluctuations wavenumber $\mathbf{q}^\delta$ and the magnetic field $\beta = \angle(\mathbf{q}^\delta, \mathbf{B})$, where $\mathbf{B} = -\mathbf{e}_z B$, and $\beta \approx 46^\circ$. The initial beam width $\rho^i = 2$ cm and $\rho^+ = \rho^i$, and distance between the emitter and scattering area, and between the receiver and the beam cross-sectional points are 50 cm. The result of the effective spectrum evaluation $S^{eff}_{nn}(\omega, \mathbf{q}^\delta)$ for different turbulence amplitudes is depicted in Figs. 3 and 4 for the cases without and with the plasma inhomogeneity effect $\frac{k_0}{L} = 0$ and $\frac{k_0}{L} = 0.04$ cm^{-2}, respectively. The turbulence amplitude is defined as $\frac{\delta n^{rms}_{\max}}{n_{\max}}$. The two plots demonstrate the comparison of the fluctuation spectrum $S_{nn}(\omega, \mathbf{q}^\delta)$ with its effective value $S^{eff}_{nn}(\omega, \mathbf{q}^\delta)$ for different turbulence amplitudes: 0%, 3%, 6%, and 10%.

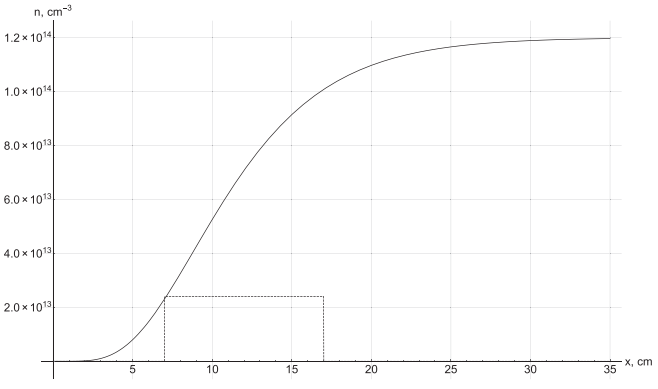

FIG. 2. Density profile—solid curve and the turbulence envelope for the turbulence amplitude $\frac{\delta n^{rms}(x)}{n_{\max}} = 0.2$—dashed curve.

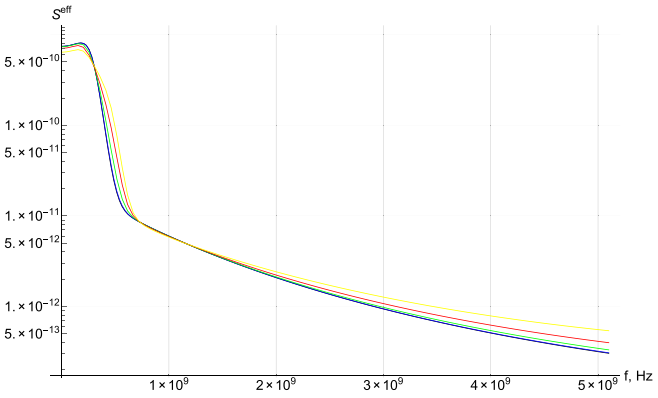

FIG. 3. Black curve (almost fully beyond the blue one) is S_{nn}; the blue, green, red, and yellow curves stand for S_{nn}^{eff} for different turbulence amplitudes: 0%, 3%, 6%, and 10%, respectively. Without considering the local plasma inhomogeneity, $\frac{k_0}{L} = 0\ \text{cm}^{-2}$.

It is seen that when the edge turbulence is absent, the effective spectrum almost coincides with the spectrum $S_{nn}(\omega, \mathbf{q}^{\delta})$, and it means that the beam angular broadening, caused only by the natural diffraction, does not play a big role for the registered signal. In the cases with turbulence, the effective spectrum distortion effect grows with the turbulence amplitude. Taking into account, the plasma inhomogeneity makes this effect only more pronounced. The relatively small impact of the plasma inhomogeneity is due to the small value of $\frac{k_0}{L}$. In the framework of the used plasma model, $\frac{k_0}{L} = 0.04\ \text{cm}^{-2}$ entails $L \approx 300$ cm. Even if this plasma is close to be homogeneous, the choice of L is limited with the applicability criterion (it is a border of applicability for the case with the 10% turbulence rate), so one should understand taking into account the plasma inhomogeneity effect as an estimate in a fairly narrow applicability domain. Both plots (3) and (4) demonstrate that the two spectra S_{nn}^{eff} and S_{nn} shapes are different. In the frequency range of $0 - 0.3$ GHz, the difference is several times; in the frequency domain range of $0.3 - 0.6$ GHz, it may reach about one order of magnitude for the high turbulence amplitudes. The effective spectrum $S_{nn}^{eff}(\omega, \mathbf{q}^{\delta})$ decrease rate is smaller than for $S_{nn}(\omega, \mathbf{q}^{\delta})$ in the area of the higher frequencies.

The spectrum contribution function $SCF(q_x, q_y, q_z)$ (35) is a normalized exponent of the quadratic form of the three wavenumber components, and the evaluation of this function provides information on the wavenumber range around $\mathbf{q}^{\delta}$ that contributes to the scattered radiation. For example, the combination $\frac{SCF(q_x,0,0)}{SCF(0,0,0)}$ is evaluated for different turbulence amplitudes together with the combination $\frac{SCF(0,0,q_z)}{SCF(0,0,0)}$ (that is independent of the turbulence) on Fig. 5 for the plasma conditions and the geometry corresponding to the evaluated spectra on Fig. 3. Under these conditions, $\frac{SCF(q_x,0,0)}{SCF(0,0,0)} = \frac{SCF(0,q_y,0)}{SCF(0,0,0)}$. It is seen that if the turbulence level is high enough, the significant beam angular broadening takes place that is expressed in the contribution to the scattered radiation from the fluctuations with a wide range of different perpendicular wave numbers compared with the vacuum probing wavenumber.

The fast particle contribution to the spectrum is significant in the high-frequency range[15] ($\gtrsim 0.5$ GHz), whereas the small frequencies carry information about the bulk ions. The spectrum shape is a function of various plasma parameters, and if all of them except for the bulk ion temperature are known, the temperature can be defined from fitting a measured spectrum by the analytical expression using the least squares fitting procedure.[19] Since the spectrum shape is distorted by the edge turbulence, using the spectrum S_{nn} for fitting experimental data instead of the effective spectrum S_{nn}^{eff} leads to an error in the defined ion temperature T_i^{fit}. In order to estimate this error for different turbulence regimes, the evaluated effective spectra S_{nn}^{eff} are fitted by $S_{nn}(T_i^{fit})$ for the conditions corresponding to the spectra S_{nn}^{eff} on Fig. 3. The results of the least squares fitting procedure are demonstrated in Fig. 6 (in the linear scale), where the dashed curves are the evaluated spectra S_{nn}^{eff} and the solid curves of the same colors are results of the fitting $S_{nn}(T_i)$. The relative values are as follows: $\frac{T_i^{fit}}{T_i} = 1.02$, 1.09, and 1.22 for the tested turbulence amplitudes 3%, 6%, and 10%, respectively, where T_i is the ion temperature used in the evaluation of the effective spectrum S_{nn}^{eff}. So, the relative error in the bulk ion

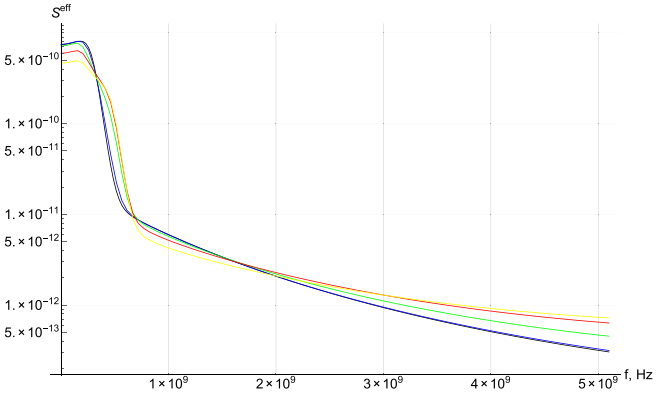

FIG. 4. Black curve is S_{nn}; the blue, green, red, and yellow curves stand for S_{nn}^{eff} for different turbulence amplitudes: 0%, 3%, 6%, and 10%, respectively. The case taking into account the local plasma inhomogeneity is $\frac{k_0}{L} = 0.04\ \text{cm}^{-2}$.

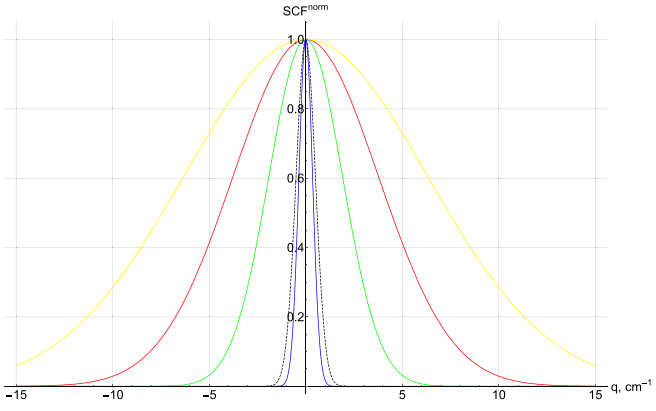

FIG. 5. Normalized spectrum contribution function, the dashed curve is $\frac{SCF(0,0,q_z)}{SCF(0,0,0)}$; the solid curves denote $\frac{SCF(q_x,0,0)}{SCF(0,0,0)}$ for the different turbulence amplitudes: the blue, green, red, and yellow curves stand for the turbulence amplitudes 0%, 3%, 6%, and 10%, respectively.

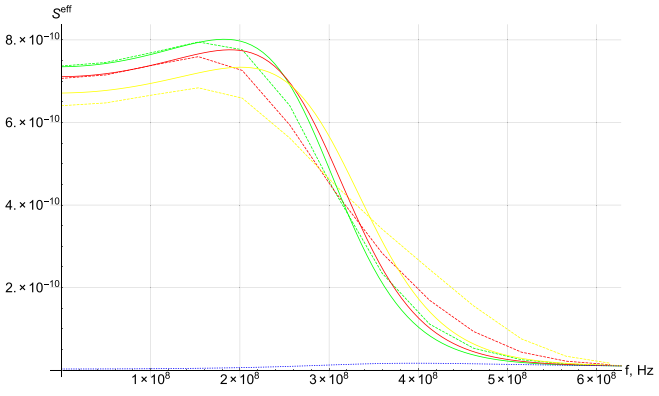

FIG. 6. Green, red, and yellow dashed curves are S_{nn}^{eff} for the different turbulence amplitudes: 3%, 6%, and 10%, respectively; the solid curves represent the fitting spectra $S_{nn}(T_i^{fit})$ with $\frac{T_i^{fit}}{T_i} = 1.02$, 1.09, and 1.22, respectively. The blue dotted curve is S_α.

temperature definition can be a few percentages or even of the order of 10% for the high turbulence level. The blue dotted curve in Fig. 6 is S_α—the component of the spectrum, which is associated with the fast particle contribution. Behavior of this function specifies the frequency range where the fast particles become the dominant to the scattered radiation. It is seen from Fig. 6 that this range starts at about 0.5 GHz.

The next numerical experiment is fulfilled for a smaller value of the angels $\psi^i = \psi^+ = 6°$, so the probing and receiving angles to the magnetic field are 84°, and it is close to perpendicular probing, $\alpha = 90°$ that leads to the scattering angle $\theta \approx 94°$ and the angle between the main resolved fluctuations wavenumber and the magnetic field $\beta \approx 70°$. The initial beam widths $\rho^+ = \rho^i = 2$ cm are the same. The comparison of the two spectra, under the different turbulence amplitudes 0%, 2%, 3%, and 6%, is shown in Figs. 7 and 8 for the conditions without and with accounting for the local density gradient $\frac{k_0}{L} = 0$ and $\frac{k_0}{L} = 0.04\ \text{cm}^{-2}$, respectively.

The very significant discrepancy between $S_{nn}^{\text{eff}}(\omega, \mathbf{q}^\delta)$ and $S_{nn}(\omega, \mathbf{q}^\delta)$ is associated with the spectrum $S_{nn}(\omega, \mathbf{q}^\delta)$ sensitivity to the very small longitudinal wavenumber q_z, and this effect is related to the

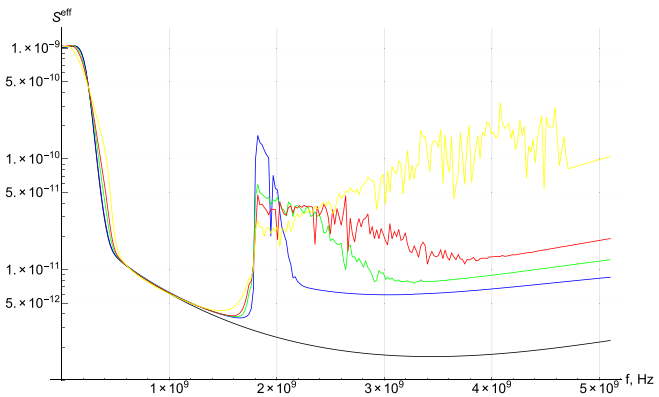

FIG. 7. Black curve is S_{nn}; the blue, green, red, and yellow curves stand for S_{nn}^{eff} for different turbulence amplitudes: 0%, 2%, 3%, and 6%, respectively. Without considering the local plasma inhomogeneity, $\frac{k_0}{L} = 0\ \text{cm}^{-2}$.

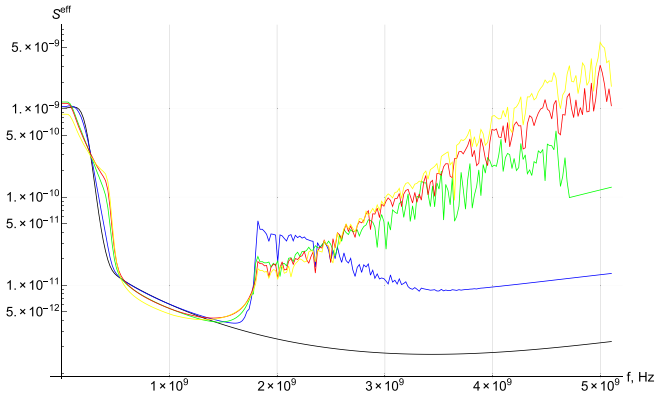

FIG. 8. Black curve is S_{nn}; the blue, green, red, and yellow curves stand for S_{nn}^{eff} for different turbulence amplitudes: 0%, 2%, 3%, and 6%, respectively. The case taking into account the local plasma inhomogeneity is $\frac{k_0}{L} = 0.04\ \text{cm}^{-2}$.

mode propagation perpendicularly to the magnetic field, which was noted in Refs. 17 and 18. The spectrum contribution function can be written as $SCF(\mathbf{q}) = SCF_\perp(q_x, q_y)SCF_\parallel(q_z)$ with the normalization $\int dq_x dq_y SCF_\perp = \int dq_z SCF_\parallel = 1$, and the plasma turbulence does not change the longitudinal part $SCF_\parallel(q_z)$, so the noticeable discrepancy between the two spectra takes place even in plasma without the turbulence. That is why a finite big enough toroidal angle is needed to avoid interference in the CTS spectrum from plasma waves propagating perpendicularly to the magnetic field.[12] This choice of the scattering angle leads to the decrease in the scattering signal; however, it allows us to diagnose the plasma ion component. Yet, there is another parameter that can be used to avoid the interference. According to Eq. (35), $SCF_\parallel(q_z)$ depends on probing beam sizes $\rho^{i,+}$. An increase in the widths $\rho^{i,+}$ leads to reduction of its angular broadening, and then, Bragg's selection rule is fulfilled for narrower wavenumber $\mathbf{q}_\parallel$ range. It should be mentioned that the spectra tail off for the higher frequencies, and the demonstrated frequency range is typical for the CTS measurements[19] and allows clearly to observe the significant discrepancy around 0.5 GHz.

The significant difference between the spectra S_{nn} and S_{nn}^{eff} in the case without the plasma turbulence is shown in Figs. 7 and 8 but does not present on Figs. 3 and 4 because the angle β is closer to 90° for the simulations corresponding to Figs. 7 and 8. Normally, the resonance peak of the spectrum, associated with the lower hybrid resonance (LHR),[18] is observed for the angles $\beta \sim 85 - 95°$, and this is correct for the turbulence spectrum S_{nn}. As it was mentioned, the effective spectrum S_{nn}^{eff} also depends on the probing and receiving beam widths, and the tested values $\rho^i = \rho^+ = 2$ cm were too small for eliminating the effect of the LHR at $\beta \approx 70°$. In order to stress the effect of the LHR influence on the effective spectrum for $\beta \approx 70°$ and the small beam width $\rho^i = \rho^+ = 2$ cm, the function $S_\parallel(\delta q_z + q_z)SCF_\parallel(q_z)$ $(S_\parallel(q_z) = \int\int dq_x dq_y S_{nn}(q_x, q_y, q_z)SCF_\perp(q_x - \delta q_x, q_y - \delta q_y))$ is illustrated in Fig. 9 for different frequencies $f = \{1.0, 1.8, 4.0\}$ GHz. It is seen that the exponential decrease in the function $SCF_\parallel(q_z)$ is not fast enough to suppress the contribution of the turbulence modes with the small toroidal wave numbers to the effective turbulence spectrum $S_{nn}^{eff} = \int dq_z S_\parallel(\delta q_z + q_z)SCF_\parallel(q_z)$ for the frequencies $f = \{1.8, 4.0\}$ GHz, whereas the contribution is negligible for $f = 1.0$ GHz that corresponds to the spectra on Figs. 7 and 8. The described effect disappears

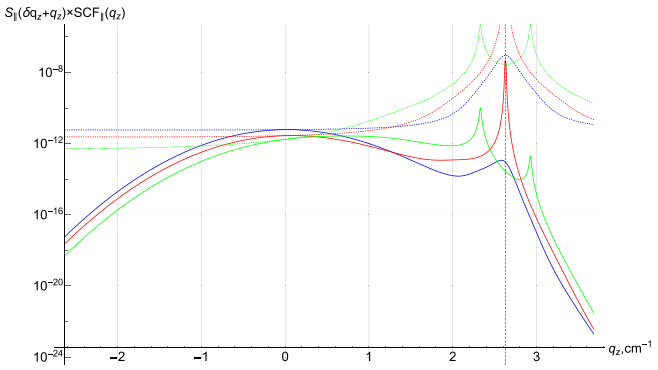

FIG. 9. Solid curves are $S_{\|}(\delta q_z + q_z)SCF_{\|}(q_z)$ dependence on the toroidal wave number q_z when $\rho^i = \rho^+ = 2$ cm, the dashed curves are $S_{\|}(\delta q_z + q_z)$, the blue curves stand for $f = 1.0$ GHz, red—$f = 1.8$ GHz and green—$f = 4.0$ GHz; the vertical dashed line specifies—δq_z.

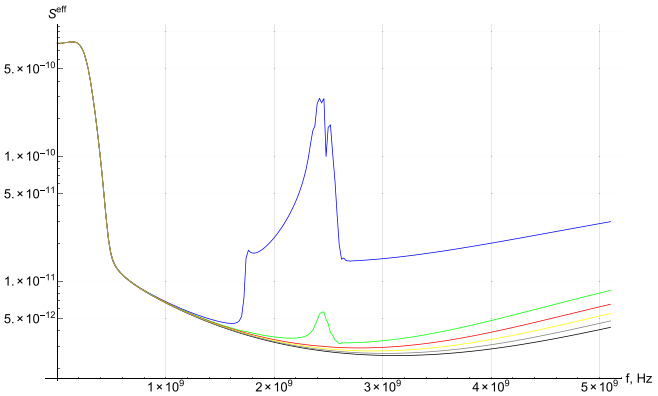

FIG. 11. Black curve is S_{nn}; the blue, green, red, yellow, and gray curves represent S_{nn}^{eff} for different probing beam sizes $\rho^i = \rho^+$: 2.0, 2.4, 2.8, 3.5, and 5.0 cm, respectively.

for the tested angle $\beta \approx 70^\circ$ if the beam widths are not that small, and the function $S_{\|}(\delta q_z + q_z)SCF_{\|}(q_z)$ is evaluated for $\rho^i = \rho^+ = 3$ cm and depicted on Fig. 10.

In order to explicitly demonstrate the effect of the interference in the CTS spectrum decrease with growing $\rho^{i,+}$, the effective spectrum $S_{nn}^{eff}(\omega, \mathbf{q}^\delta)$ is evaluated for different values $\rho^+ = \rho^i \in \{2.0, 2.4, 2.8, 3.5, 5.0\}$ cm, see Fig. 11. There are different systems of the microwave power generation at different machines. The standard width of a probing beam is typically a few centimeters, for instance, $\rho^+ = 2$ cm for the receiver prototype for future CTS at ITER.[12] The parameters of the simulation: $\psi^i = \psi^+ = 6^\circ$ and the poloidal angle $\alpha = 45^\circ$, so $\theta \approx 133^\circ$ and $\beta \approx 73^\circ$, the plasma is without the turbulence and the local density gradient . It is seen from Fig. 6 that $S_{nn}^{eff}(\omega, \mathbf{q}^\delta)$ is very sensitive to the initial beam widths. Then, the probing beam width is also an instrument to destroy the interference between the elongated in the toroidal direction electron fluctuations.

V. CONCLUSION

It was clear that finite angular broadening of a probing beam can be quite big due to the plasma edge turbulence, and it leads to contribution to the scattered signal from various wave numbers in the

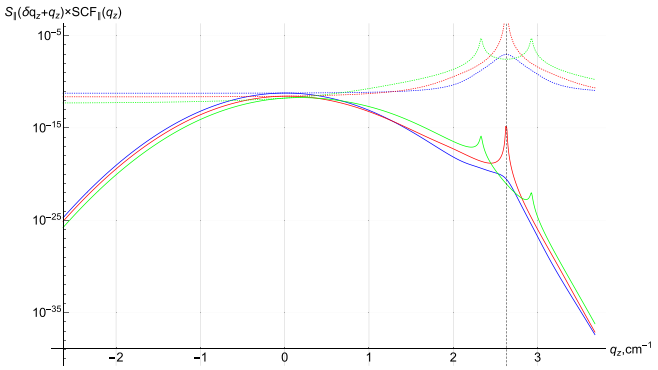

FIG. 10. Solid curves are $S_{\|}(\delta q_z + q_z)SCF_{\|}(q_z)$ dependence on the toroidal wave number q_z when $\rho^i = \rho^+ = 3$ cm, the dashed curves are $S_{\|}(\delta q_z + q_z)$, the blue curves stand for $f = 1.0$ GHz, red—$f = 1.8$ GHz, and green—$f = 4.0$ GHz; the vertical dashed line specifies—δq_z.

vicinity of the general one $\mathbf{q}^\delta$. This effect was analyzed explicitly in this work. This effect leads to the consideration of the effective turbulence spectrum instead of the turbulence spectrum itself in the expression for the registered signal. It is numerically demonstrated that the difference between the spectra grows with increasing edge turbulence level. Various frequency domains demonstrate different relations between $S_{nn}^{eff}(\omega, \mathbf{q}^\delta)$ and $S_{nn}(\omega, \mathbf{q}^\delta)$. The effective spectrum is relatively mitigated for the small frequencies about $0 - 0.3$ GHz, and this frequency range is normally associated with the electrons and bulk ions, whereas the contribution of the fast particles is dominant in the tail of the spectrum for frequencies $\gtrsim 0.5$ GHz. In the domain of higher frequencies, $S_{nn}^{eff}(\omega, \mathbf{q}^\delta)$ mostly surpasses $S_{nn}(\omega, \mathbf{q}^\delta)$, and the relative increase in effective spectrum is especially pronounced in the range of $0.3 - 0.6$ GHz.

Since not only the angular but also the spatial beam broadening takes place, the effect of the local plasma inhomogeneity can also change the results of the CTS measurements. This contribution is also taken into account in the definition of the effective turbulence spectrum, and a criterion of the analytical applicability is provided. Numerical simulations accounting for the effect of the local inhomogeneity show that this effect slightly increases the difference between $S_{nn}^{eff}(\omega, \mathbf{q}^\delta)$ and $S_{nn}(\omega, \mathbf{q}^\delta)$.

The numerical simulations with a small toroidal angle $\psi^{i,+} = 6^\circ$ demonstrated that there is an enormous contribution to the CTS signal from the electron fluctuations with small $\mathbf{q}_{\|}$ and different from the main resolved according to Braggs' rule wave number $\delta\mathbf{q}_{\|}$. This result is in agreement with previous studies,[18] and the turbulence spectrum $S_{nn}(\omega, \mathbf{q}^\delta)$ is still affected by the LHR for the almost perpendicular $\mathbf{q}^\delta$ to the magnetic field, but the LHR can influence on the effective spectrum $S_{nn}^{eff}(\omega, \mathbf{q}^\delta)$ even for $\beta \approx 70^\circ$ if the probing and receiving beam widths are not big enough. It is demonstrated that it is possible to mitigate this effect by choosing a big enough probing beam width.

The influence of the plasma edge turbulence on the CTS spectrum is described analytically and numerically. An estimate of the possible error in the bulk ion temperature definition is provided, and the relative error can be 10% or lesser depending on a turbulence scenario. A detailed analysis of the importance of the registered spectrum correction due to the edge turbulence is yet to be considered; strictly

speaking, it should be done for determining all the plasma and the fast particle parameters that are theoretically possible to be extracted from the CTS measurements.

Conflict of Interest

The authors have no conflicts to disclose.

Author Contributions

Pavel Tretinnikov: Formal analysis (lead); Investigation (lead); Software (lead); Validation (equal); Visualization (lead); Writing – original draft (lead). **Evgeniy Gusakov:** Conceptualization (equal); Methodology (equal); Supervision (equal); Validation (equal); Writing – review & editing (equal). **Stephane Heuraux:** Conceptualization (equal); Methodology (equal); Supervision (equal); Validation (equal); Writing – review & editing (equal).

DATA AVAILABILITY

The data that support the findings of this study are available within the article.

APPENDIX: DERIVATION OF THE EXPRESSION FOR NON-LINEAR CURRENT

Derivation of the source current in the framework of the cold fluid model is described in this Appendix section.

The expression for the bilinear current (multiplied by $\mathbf{e}^+$) in general terms reads as

$$\mathbf{e}^+\mathbf{j}^{nl} = \mathbf{e}^+ e\left[n_e\mathbf{u}^{nl} + n^\delta\mathbf{u}^i + n^i\mathbf{u}^\delta\right], \tag{A1}$$

where $\mathbf{u}^i$ and n^i are linear perturbations of the electron velocity and density caused by a probing wave. $\mathbf{E}^i$, $\mathbf{u}^\delta$, and n^δ are analogous linear perturbations associated with the fluctuations, $\mathbf{u}^{nl}$ is a quadratic perturbation—product of the probing wave interaction with the fluctuations. Linearization of the motion equation set and the charge balance equation (in the Fourier transformed form) gives

$$\mathbf{u}^i = \mathbf{e}_\mu \frac{ie}{m_e\omega^i}\zeta_\mu E^i, \tag{A2}$$

$$n^i = \frac{n_e}{\omega^i}k^i_\mu u^i_\mu. \tag{A3}$$

Keeping all the quadratic terms in the motion equation set, we have

$$u^{nl}_\mu = \frac{ie}{cm_e\omega^s}e_{\mu jk}\left[u^i_j B^\delta_k + u^\delta_j\frac{c}{\omega^i}e_{knm}k^i_n\left(\mathbf{e}_m\mathbf{e}^i\right)E^i\right], \tag{A4}$$

where e_{ijk} is the Levi-Civita symbol. Finally, making use of the equality $e_{ijk}e_{i\xi\xi'} = \delta_{j\xi}\delta_{k\xi'} - \delta_{j\xi'}\delta_{k\xi}$ and performing the inverse Fourier transform, we end up with

$$\mathbf{e}^+\mathbf{j}^{nl}(t,\mathbf{r}) = i\frac{e^2}{m_e}\frac{n_e}{\omega^i}\chi_\xi f^\delta_\xi(t,\mathbf{r})e^{-i\omega^i t}E^i(\mathbf{r}). \tag{A5}$$

This expression can be used for any probing wave polarization $\mathbf{e}^i$; also, one should keep in mind that the source current $\mathbf{j}^{nl}$ can be expressed in various ways due to the linear relations between the fluctuating characteristics, and the expression in the presented form is convenient for analyzing the scattering process for a certain dominant type of the fluctuations.

REFERENCES

[1]E. Gusakov and A. Surkov, Plasma Phys. Controlled Fusion **46**, 1143 (2004).
[2]S. B. Korsholm, H. Bindslev, V. Furtula, F. Leipold, F. Meo, P. K. Michelsen, D. Moseev, S. K. Nielsen, M. Salewski, and M. Stejner, Nucl. Instrum. Methods Phys. Res., Sect. A **623**, 677–680 (2010).
[3]E. V. Sysoeva, F. da Silva, E. Z. Gusakov, S. Heuraux, and A. Popov, Nucl. Fusion **55**(3), 033016 (2015).
[4]P. Tretinnikov, E. Gusakov, and S. Heuraux, Plasma Phys. Controlled Fusion **63**, 085003 (2021).
[5]N. Bertelli, G. J. Kramer, and E. J. Valeo, Plasma Phys. Controlled Fusion **61**, 105018 (2019).
[6]A. Snicker, E. Poli, O. Maj, L. Guidi, A. Köhn, H. Weber, G. D. Conway, M. Henderson, and G. Saibene, Plasma Phys. Controlled Fusion **60**, 014020 (2018).
[7]O. Chellaï, S. Alberti, I. Furno, T. Goodman, A. Koehn, L. Figini, D. Ricci, L. Hizanidis, P. Papagiannis, C. Tsironis, and the TCV Team, EPJ Web Conf. **157**, 03008 (2017).
[8]C. Tsironis, A. G. Peeters, H. Isliker, D. Strintzi, I. Chatziantonaki, and L. Vlahos, Phys. Plasmas **16**, 112510 (2009).
[9]H. Bindslev, Plasma Phys. Controlled Fusion **33**, 1775 (1991).
[10]H. Bindslev, Plasma Phys. Controlled Fusion **35**, 1615–1640 (1993).
[11]R. E. Slusher and C. M. Surko, Phys. Fluids **23**, 472 (1980).
[12]S. B. Korsholm, EPJ Web Conf. **203**, 03002 (2019).
[13]S. M. Rytov and Y. A. Kravtsov, *V I Tatarskii" Principles of Statistical Radiophysics"* (Springer-Verlag, Berlin, 1989), Vol. 3.
[14]A. D. Piliya and A. Y. Popov, Plasma Phys. Controlled Fusion **44**, 467–474 (2002).
[15]D. P. Hutchinson, K. L. Vander Sluis, J. Sheffield, and D. J. Sigmar, Rev. Sci. Instrum. **56**, 1075 (1985).
[16]J. D. Gaffey, Plasma Phys **16**, 149 (1976).
[17]L. Vahala, G. Vahala, and D. J. Sigmar, Nucl. Fusion **26**, 51 (1986).
[18]J. Rasmussen, M. Stejner, T. Jensen, E. B. Klinkby, S. B. Korsholm, A. W. Larsen, F. Leipold, S. K. Nielsen, and M. Salewski, Nucl. Fusion **59**, 096051 (2019).
[19]S. K. Nielsen, H. Bindslev, L. Porte, J. A. Hoekzema, S. B. Korsholm, F. Leipold, F. Meo, P. K. Michelsen, S. Michelsen, J. W. Oosterbeek, E. L. Tsakadze, G. Van Wassenhove, E. Westerhof, and P. Woskov, Phys. Rev. E **77**, 016407 (2008).